LETTERS

The role of terrestrial plants in limiting atmospheric CO_2 decline over the past 24 million years

Mark Pagani[1], Ken Caldeira[2], Robert Berner[1] & David J. Beerling[3]

Environmental conditions during the past 24 million years are thought to have been favourable for enhanced rates of atmospheric carbon dioxide drawdown by silicate chemical weathering[1–7]. Proxy records indicate, however, that the Earth's atmospheric carbon dioxide concentrations did not fall below about 200–250 parts per million during this period[8]. The stabilization of atmospheric carbon dioxide concentrations near this minimum value suggests that strong negative feedback mechanisms inhibited further drawdown of atmospheric carbon dioxide by high rates of global silicate rock weathering. Here we investigate one possible negative feedback mechanism, occurring under relatively low carbon dioxide concentrations and in warm climates, that is related to terrestrial plant productivity and its role in the decomposition of silicate minerals[9–11]. We use simulations of terrestrial and geochemical carbon cycles and available experimental evidence to show that vegetation activity in upland regions of active orogens was severely limited by near-starvation of carbon dioxide in combination with global warmth over this period. These conditions diminished biotic-driven silicate rock weathering and thereby attenuated an important long-term carbon dioxide sink. Although our modelling results are semi-quantitative and do not capture the full range of biogeochemical feedbacks that could influence the climate, our analysis indicates that the dynamic equilibrium between plants, climate and the geosphere probably buffered the minimum atmospheric carbon dioxide concentrations over the past 24 million years.

Alkenone-based proxy records[8] indicate that atmospheric carbon dioxide (CO_2) concentrations ranged between 1,000 and 1,500 parts per million (p.p.m.) from about 45 to 34 million years (Myr) ago (the middle to late Eocene epoch), decreased from ~34 to 24 Myr ago (the Oligocene epoch), and approached modern levels by ~24 Myr ago (the early Miocene epoch) (Fig. 1a). Long-term declines in ocean temperatures from the early Eocene leading to the appearance of small Antarctic ice sheets by the late Eocene[12], and a striking shift to colder high-latitude climates at ~34 Myr ago, are climate trends consistent with these CO_2 records (Fig. 1b). In contrast, the final 24 Myr of the Cenozoic era—a time known for periods of both global warmth and substantial ice accumulation—was characterized by relatively low atmospheric CO_2 concentrations[8]. Despite very different assumptions and uncertainties, this CO_2 history for the past 24 Myr or so is reinforced by other CO_2 estimates, including ocean pH reconstructions using the boron isotope composition of foraminifera[13] (Fig. 1a), and low but variable CO_2 values based on the stomatal indices of fossil leaves[14].

The drop in atmospheric CO_2 concentrations from ~50 to 24 Myr ago (Fig. 1a) was driven by a decrease in geologic CO_2 degassing and/or enhanced chemical weathering of silicate rocks[15]. Although there is no consensus regarding Cenozoic CO_2 degassing rates[16–19], most spreading-rate estimates suggest that seafloor production (and CO_2 input) declined slightly[17,18] or remained constant over the past 65 Myr (ref. 19), with no evidence for distinct changes in spreading rates during the Eocene or the Oligocene. In contrast, physical weathering rates of silicate rocks accelerated with surface uplift and erosion, as inferred by an increase in the global sedimentation rate of sandstones and shales with time[15].

Orogenic reconstructions emphasize the past 65 Myr as a time of active tectonism (Fig. 1a). Himalayan surface uplift includes Andean-style ranges by ~60 Myr ago[1], near-modern elevations for some regions of southern Tibet by the Oligocene[2,3], and large changes in topographic relief and rates of denudation during the late Oligocene and Miocene[1]. Andean surface uplift began sometime in the early Oligocene, with crustal thickening and exhumation during the late Oligocene[4,5] and surface uplift in the late Miocene[6]. Finally, exhumation of the massive New Guinea arc occurred during the middle Miocene[7], while surface uplift of the southern Alps of New Zealand was delayed until the latest Miocene to early Pliocene epoch[5].

The decline in CO_2 at ~34 Myr ago required a small (that is, less than 0.01 gigatonnes of carbon per year) but sustained imbalance in the carbon cycle[20]. A striking feature of Cenozoic tectonic activity is the scale of surface uplift and denudation of recent orogens during the past 24 Myr, as well as a lack of evidence for increased metamorphic and volcanic degassing[21]. The current paradigm of climate stability applied in all geochemical carbon simulations assumes a strong CO_2-driven weathering feedback that changes with temperature and soil CO_2 concentration and mitigates large changes in CO_2 over a few million years[15]. Indeed, the small variance in the mean atmospheric CO_2 trend for the past ~650,000 years requires a strong weathering feedback for the observed balance of carbon fluxes[22]. Rates of silicate weathering are modulated by the supply of weatherable minerals and by reaction kinetics, often ascribed to hydrology and temperature[23], with high chemical weathering rates observed in wet, warm regions experiencing active orogenesis. Accordingly, enhanced low-latitude tectonic activity and relative global warmth during the past 24 Myr should have led to a significant long-term imbalance in carbon fluxes and CO_2 drawdown. Contrary to this expectation, atmospheric CO_2 concentrations did not plunge to extremely low values (Fig. 1a), despite changes in climate and the creation of environments that rapidly consume atmospheric CO_2. To stabilize atmospheric CO_2 near its minimum value for over 20 Myr would necessitate either fortuitously balancing multi-million-year carbon fluxes (an unrealistic scenario given the magnitude of the carbon fluxes involved), or negative feedback mechanisms that opposed higher rates of silicate–chemical weathering and further CO_2 decline during the warmth of the early to middle Miocene.

Here, we identify one overlooked negative feedback mechanism occurring under relatively low CO_2 and in warm climates, related to

[1]Department of Geology and Geophysics, Yale University, New Haven, Connecticut 06520, USA. [2]Department of Global Ecology, Carnegie Institution of Washington, Stanford, California 94305, USA. [3]Department of Animal and Plant Sciences, University of Sheffield, Sheffield S10 2TN, UK.

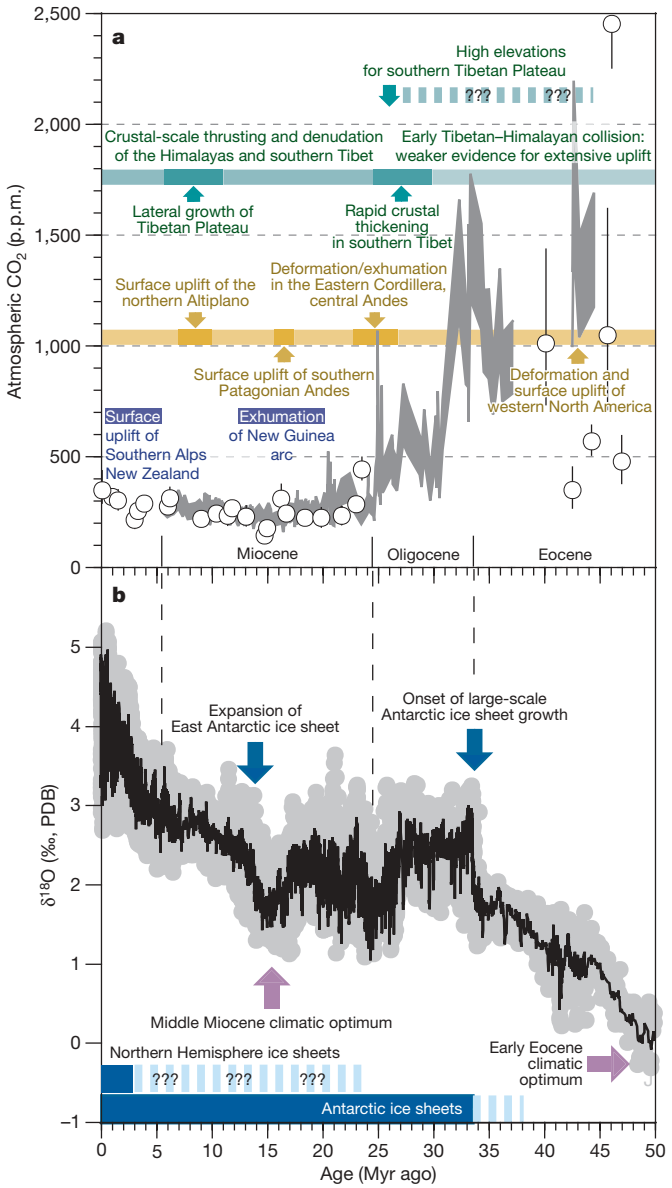

Figure 1 | The Earth's CO_2, tectonic and climatic history over the past 50 Myr. **a**, Proxy records of long-term changes in atmospheric CO_2 concentration. Shaded bands represent a range of alkenone-based atmospheric CO_2 estimates[8]. Open circles represent CO_2 estimates from boron isotope–pH reconstructions[13]. **b**, Long-term $\delta^{18}O$ record from benthic foraminifera[12]. p.p.m., parts per million. PDB, Pee Dee belemnite standard.

terrestrial plant productivity and its role in the decomposition of silicate minerals. The mechanistic basis for the relationship between terrestrial plant activity and chemical weathering is well understood[9–11]. Rooted vascular plants, and their belowground mycorrhizal fungal partners, accelerate rates of chemical weathering by a factor of 1.5 to <10 through a variety of mechanisms associated with recently fixed organic carbon fluxes exported belowground. Biologically enhanced weathering occurs (1) when roots mechanically fracture minerals and increase the surface area available for dissolution, (2) as soil solution pH is lowered by the introduction of root-respired CO_2, organic carbon oxidation, organic acids and proton exchange during nutrient uptake, and (3) through chelation by organic ligands, secreted from rootlets and their associated microorganisms that act to lower the activity of metals and saturation states, leading to enhanced mineral dissolution and nutrient supply for plant growth. Further, canopy transpiration influences the rates of chemical reactions and microbial activity by increasing the residence time of unsaturated soil water. Accordingly, global rates of silicate chemical weathering are linked to biologically enhanced weathering through the health of terrestrial ecosystems.

The dominant plants associated with high silicate–chemical weathering rates in upland regions use the C_3 photosynthetic pathway. However, the efficacy of C_3 photosynthesis is compromised under specific environmental conditions because the primary enzyme catalysing carbon fixation (Rubisco; ribulose-1,5-bisphosphate carboxylase/oxygenase) also reacts with diatomic oxygen, resulting in photorespiratory release of CO_2 and lower photosynthetic rates (as much as 30%–40% below modern CO_2 levels)[24]. Photorespiration rates are amplified under low atmospheric CO_2/O_2 ratios, when O_2 significantly competes for the acceptor molecule ribulose bisphosphate, and higher temperatures, which alter both the solubility of O_2 relative to CO_2 and the specificity of Rubisco in favour of O_2 (Fig. 2). Both environmental effects on the oxygenase activity of Rubisco are greatly diminished at high CO_2 by increased competitive inhibition of O_2 for ribulose bisphosphate[25]. These fundamental biochemical properties of leaves indicate that the photorespiratory burden of vegetation probably increased as CO_2 began to decline in

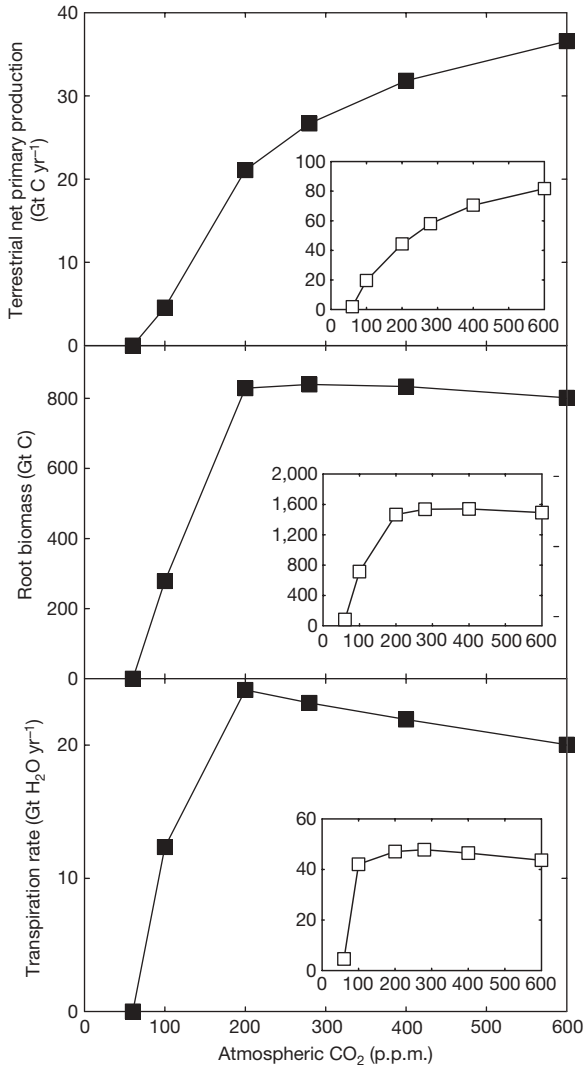

Figure 2 | Simulated dependence of vegetation activity on atmospheric CO_2 concentrations. All simulations used a dynamic global vegetation model and a pre-industrial climate. The main panels show global tropical forest responses; insets (axes units as for main panels) show the global terrestrial biosphere responses. The tropical forest canopy transpiration declines as atmospheric CO_2 concentrations rise above 200 p.p.m. because leaf area index is maximal and CO_2 induces stomatal closure. Gt, gigatonnes.

response to increased chemical weathering from orogenic uplift, especially during episodes of global warmth. Terrestrial vegetation activity would have decreased, weakening its feedback on silicate-rock weathering and offsetting the effect of orogenic uplift on the decrease of atmospheric CO_2.

We investigated the significance of this proposed feedback mechanism on ecosystem properties through simulations with a dynamic global vegetation model that includes representation of the above- and belowground carbon and nitrogen cycles at atmospheric CO_2 concentrations between 50 and 500 p.p.m. (ref. 26). Our results indicate that under present-day climate conditions, the tropical and global forest primary production and root biomass—two key ecosystem properties that enhance soil-weathering rates—decline abruptly at CO_2 concentrations below about 200 p.p.m. (Fig. 2). Similarly, global and tropical forest canopy transpiration rates are strongly diminished by falling atmospheric CO_2 concentrations. These results are supported by independent global-scale simulations of Miocene vegetation showing that forest productivity, particularly in warm tropical regions where photorespiration rates are highest, is strongly constrained by atmospheric CO_2 concentrations of 200–280 p.p.m. (ref. 26). As the minimum level of CO_2 (the level required to sustain C_3 plant growth and reproduction at the ecosystem level) is approached, key mechanisms that accelerate chemical weathering in actively weathering regions begin to slow, weakening the strength of a biologically mediated sink for CO_2 (Fig. 2).

The well-documented loss of forest cover and expansion of C_3 grasslands during the latest Oligocene to early Miocene[27] attest to environmental conditions unfavourable to forest productivity. Grasses have shallow root systems and symbiosis with arbuscular mycorrhizal fungi that do not secrete the low-molecular-weight organic acids involved in biotic weathering by ectomycorrhizal-dominated forests[28]. Thus, this widespread replacement of forests by C_3 grasslands including grasses with the carbon-concentrating C_4 photosynthetic pathway probably further weakened the biotic weathering feedback.

The minimum CO_2 concentration that is critical for the natural ecosystem weathering feedback is not precisely known and its absolute value is likely to have changed with global mean temperature via its influence on respiration rates. Evidence from experiments and ice-core records suggest it lies between $\geq$100 and $\leq$190 p.p.m. during cooler global temperatures of the Pleistocene. The lower value is consistent with the minimum CO_2 concentration required for successful reproduction of a subtropical herb (tobacco needs ~100 p.p.m.; ref. 29). The upper estimate derives from Pleistocene ice-core studies that show that terrestrial vegetation repeatedly experienced and survived atmospheric CO_2 concentrations of ~180 p.p.m. over the last 650 kyr (ref. 22). This upper level is consistent with experimental results obtained from tropical and desert ecosystems in the Biosphere II facility in Oracle, Arizona, USA, that indicate an approximate ecological compensation point (defined as when net ecosystem exchange approaches zero) of 190 p.p.m. CO_2 (ref. 30). Given the influence of temperature on photorespiration rate, the ecological compensation point during warm intervals was probably achieved at higher CO_2 concentrations.

Geochemical carbon cycle models assume that C_3 plant growth promotes silicate-rock weathering even as the atmospheric CO_2 concentration approaches zero[15]. We evaluated the significance of including a more appropriate minimum CO_2 concentration for ecosystem weathering in a carbonate–silicate model by modifying the relationship between terrestrial primary productivity and atmospheric CO_2 using a well-established formulation for the effect of plants on soil CO_2 (see Methods Summary). Factors such as mountain uplift allow rock to weather more easily, so we introduce a dimensionless 'weatherability index' to represent the factor by which silicate-rock weathering is accelerated per unit area at constant atmospheric CO_2 (see Methods Summary). Figure 3 shows that as rocks weather more easily (owing to surface uplift, for example), atmospheric CO_2 decreases towards the critical CO_2 threshold below which plant activity does not contribute to enhanced silicate-rock weathering. As that threshold is approached, CO_2 drawdown due to biological weathering is attenuated, limiting the lower bound that CO_2 can fall to, and stabilizing atmospheric CO_2.

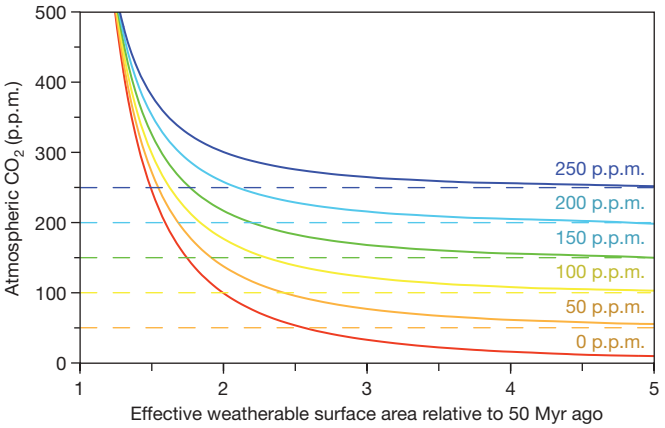

Figure 3 | Atmospheric CO_2, critical thresholds, and plant weathering. Atmospheric CO_2 predictions for critical CO_2 values ranging from 250 p.p.m. to 0 p.p.m. (see Methods Summary for details). Factors including the uplift and denudation of the Himalayas, Andes and New Guinea increased physical erosion and increased the amount of reactive mineral surface area exposed to chemical weathering. As conditions change and rocks weather more easily, the response of terrestrial plants helps buffer atmospheric CO_2 concentration above the critical threshold for vigorous plant growth.

Our results for a range of CO_2 thresholds and availability of weatherable minerals (Fig. 3) show that critical CO_2 levels between ~150 and 250 p.p.m. effectively dampen CO_2 variability and yield CO_2 concentrations consistent with the lowest values observed for the past 24 Myr (Fig. 1a). Ecological CO_2 thresholds between about 24 and 5 Myr ago were probably higher than those during the Pleistocene, when healthy plant ecosystems are associated with CO_2 concentrations of ~190 p.p.m. However, these differences are anticipated, given that warmer-than-modern Neogene temperatures probably increased photorespiration rates and raised minimum CO_2 levels.

We recognize that our modelling results are semi-quantitative and do not capture the full range of biogeochemical feedbacks that could influence climate as CO_2 declines. For example, ecosystem turnover or demise due to CO_2 stress could affect erosion rates, soil stability, rock exposure, regional changes in albedo, and influence weathering rates and changes in CO_2. More elaborate carbon-cycle and climate-system feedbacks could potentially be determined using detailed biogeochemical modelling, but the present work clearly identifies the first-order response of terrestrial C_3 ecosystems to declining CO_2 levels and rising photorespiration rates as a severe reduction in the influence of plants on rock weathering and continued CO_2 drawdown. Therefore, we conclude that land plants strongly attenuated long-term CO_2 variability and helped prevent the onset of severe icehouse conditions during tectonically active periods of the Neogene. Ecological CO_2 thresholds are a fundamental component of long-term carbon-cycle dynamics, and are needed to explain the relative constancy of atmospheric CO_2 in the face of climate and tectonic change over at least the past 24 Myr.

METHODS SUMMARY

Vegetation modelling. Leaf-scale and global-scale simulations of the sensitivity of vegetation processes to atmospheric CO_2 and climate were performed with a mechanistic biochemical model of Rubisco kinetics and a global dynamic vegetation model, respectively. Equilibrium global simulations (500 years) were undertaken at specific atmospheric CO_2 concentrations using monthly pre-industrial surface climatology (monthly fields of temperature, precipitation and humidity) with a 2.5° × 2.5° (latitude × longitude) spatial resolution.

Land-plants and silicate-rock weathering. The silicate-rock weathering rate ($f_{sw,\,50\,Myr}$) is represented as[31]:

$$f_{sw,\,50\,Myr} = k_{50\,Myr} \times (f_{land\ plants})^{0.4} \quad (1)$$

where $f_{land\ plants}$ represents the effect of land plants on soil CO_2 levels and $k_{50\,Myr}$ represents all other factors influencing silicate-rock weathering rates (assumed constant).

A formulation for the effect of land plants on soil CO_2 levels for different critical CO_2 levels below which plant activity does not contribute to enhanced silicate-rock weathering (R_{crit})[32] is expressed as:

$$f_{land\ plants,\ R_{crit}} = \left[\frac{R_{CO_2} - R_{crit}}{(R_{half} - R_{crit}) + (R_{CO_2} - R_{crit})}\right]\left(1 - \frac{1}{R_{soil,\,0}}\right) + \left(\frac{R_{CO_2}}{R_{soil,\,0}}\right) \quad (2)$$

where R_{CO_2} is the ratio of ancient atmospheric CO_2 relative to the pre-industrial CO_2 level. R_{half} is the atmospheric CO_2 level at which plants produce half of their maximum effect on silicate weathering; $R_{soil,\,0}$ is the ratio of soil CO_2 to pre-industrial atmospheric CO_2.

We adopt a $R_{soil,\,0}$ value of 10 (ref. 32) and assume $R_{half} = 2R_{CO_2}$. For each value of R_{crit}, we identify the value of $k_{50\,Myr}$ that the same silicate-rock weathering rate produced when R_{CO_2} is at a value of 1,500 p.p.m., and denote it $k_{50\,Myr,\,Rcrit}$. We then write the equation:

$$f_{sw,\,50\,Myr} = A_{rel} \times k_{50\,Myr,\,R_{crit}} \times (f_{land\ plants,\,R_{crit}})^{0.4} \quad (3)$$

where A_{rel} represents the weatherable mineral surface area relative to that at 50 Myr ago. For Fig. 3, the value of A_{rel} was increased to represent the increase in reactive silicate-mineral surface area and atmospheric R_{CO_2} was solved by substituting equation (2) into equation (3).

Full Methods and any associated references are available in the online version of the paper at www.nature.com/nature.

Received 16 February; accepted 29 April 2009.

1. Chung, S.-L. *et al.* Tibetan tectonic evolution inferred from spatial and temporal variations in post-collisional magmatism. *Earth Sci. Rev.* **68,** 173–196 (2005).
2. Rowley, D. B. & Currie, B. S. Palaeo-altimetry of the late Eocene to Miocene Lunpola basin, central Tibet. *Nature* **439,** 677–681 (2006).
3. DeCelles, P. G. *et al.* High and dry in central Tibet during the Late Oligocene. *Earth Planet. Sci. Lett.* **253,** 389–401 (2007).
4. Gillis, R. J., Horton, B. K. & Grove, M. Thermochronology, geochronology, and upper crustal structure of the Cordillera Real: implications for Cenozoic exhumation of the central Andean plateau. *Tectonics* **25,** doi:10.1029/2005TC001887 (2006).
5. Blisniuk, P. M. & Stern, L. A. Stable isotope paleoaltimetry: a critical review. *Am. J. Sci.* **305,** 1033–1074 (2005).
6. Garzione, C. N., Molnar, P., Libarkin, J. C. & MacFaden, B. J. Rapid late Miocene rise of the Bolivian altiplano: evidence for removal of mantle lithosphere. *Earth Planet. Sci. Lett.* **241,** 543–556 (2006).
7. Reusch, D. N. & Maasch, K. A. in *Tectonic Boundary Conditions for Climate Reconstruction* (eds Crowley, T. J. & Burke, K. C.) 261–276 (Oxford Monographs on Geology and Geophysics, No. 38, Oxford University Press, 1998).
8. Pagani, M., Zachos, J. C., Freeman, K. H., Tipple, B. & Bohaty, S. Marked decline in atmospheric carbon dioxide concentrations during the Paleogene. *Science* **309,** 600–603 (2005).
9. Moulton, K. L., West, J. & Berner, R. A. Solute flux and mineral mass balance approaches to the quantification of plant effects on silicate weathering. *Am. J. Sci.* **300,** 539–570 (2000).
10. Andrews, J. A. & Schlesinger, W. H. Soil CO_2 dynamics, acidification and chemical weathering in a temperate forest with experimental CO_2 enrichment. *Glob. Biogeochem. Cycles* **15,** 149–162 (2001).
11. Berner, E. K., Berner, R. A. & Moulton, K. L. Plants and mineral weathering: present and past. *Treatise Geochem.* **5,** 169–188 (2003).
12. Zachos, J., Pagani, M., Sloan, L., Thomas, E. & Billups, K. Trends, rhythms, and aberrations in global climate: 65 Ma to present. *Science* **292,** 686–693 (2001).
13. Pearson, P. N. & Palmer, M. R. Middle Eocene seawater pH and atmospheric carbon dioxide concentrations. *Science* **284,** 824–826 (1999).
14. Kürschner, W. M., Kvacek, Z. & Dilcher, D. L. The impact of Miocene atmospheric carbon dioxide on climate and the evolution of terrestrial ecosystems. *Proc. Natl Acad. Sci. USA* **105,** 449–453 (2008).
15. Berner, R. A. & Kothavala, Z. GEOCARB III: a revised model of atmospheric CO_2 over Phanerozoic time. *Am. J. Sci.* **301,** 182–204 (2001).
16. Cogné, J. & Humler, E. Trends and rhythms in global seafloor generation rate. *Geochem. Geophys. Geosyst.* **7,** doi:10.1029/2005GC001148 (2004).
17. Engebretson, D. C., Kelley, K. P., Cashman, H. J. & Richards, M. A. 180 million years of subduction. *Geol. Soc. Am. Today* **2,** 93–95 (1992).
18. Lowenstein, T. K., Timofeff, M. N., Brennan, S. T., Hardie, L. A. & Demicco, R. V. Oscillations in Phanerozoic seawater chemistry: evidence from fluid inclusions. *Science* **294,** 1086–1088 (2001).
19. Rowley, D. B. Rate of plate creation and destruction: 180 Ma to present. *Geol. Soc. Am. Bull.* **114,** 927–933 (2002).
20. Kerrick, D. M. & Caldeira, K. Metamorphic CO_2 degassing from orogenic belts. *Chem. Geol.* **145,** 213–232 (1998).
21. Kerrick, D. M. & Caldeira, K. Was the Himalayan orogen a climatically significant coupled source and sink for atmospheric CO_2 during the Cenozoic? *Earth Planet. Sci. Lett.* **173,** 195–203 (1999).
22. Zeebe, R. E. & Calderia, K. Close mass balance of long-term carbon fluxes from ice-core CO_2 and ocean chemistry records. *Nature Geosci.* doi:10.1038/ngeo185 (2008).
23. West, J., Galy, A. & Bickle, M. Tectonic and climatic controls on silicate weathering. *Earth Planet. Sci. Lett.* **235,** 211–228 (2005).
24. Pearcy, R. W. & Ehleringer, J. Comparative ecophysiology of C_3 and C_4 plants. *Plant Pop. Biol.* **7,** 1–13 (1984).
25. Ehleringer, J. R., Cerling, T. E. & Helliker, B. R. C_4 photosynthesis, atmospheric CO_2, and climate. *Oecologia* **112,** 285–299 (1997).
26. Beerling, D. J. & Woodward, F. *Vegetation and the Terrestrial Carbon Cycle; Modelling the First 400 Million Years* (Cambridge University Press, 2001).
27. Jacobs, B. F., Kingston, J. D. & Jacobs, L. L. The origin of grass-dominated ecosystems. *Ann. Missouri Bot. Garden* **86,** 90–643 (1999).
28. Taylor, L. L. *et al.* Biological weathering and the long-term carbon cycle: integrating mycorrhizal evolution and function into the current paradigm. *Geobiology* **7,** 171–191 (2009).
29. Campbell, C. D., Sage, R. F., Kocacinar, F. & Way, D. A. Estimation of the whole-plant CO_2 compensation point of tobacco (*Nicotiana tabacum* L.). *Glob. Change Biol.* **11,** 1956–1967 (2005).
30. Lin, G. *et al.* Ecosystem carbon exchange in two terrestrial ecosystem mesocosms under changing atmospheric CO_2 concentrations. *Oecologia* **119,** 97–108 (1999).

Supplementary Information is linked to the online version of the paper at www.nature.com/nature.

Acknowledgements Conversations with C. Garzione, M. Hren. J. Berry, and C. Osborne were greatly appreciated. This work was supported, in part, by NSF grant OCE-0095734 (to M.P.) and DOE grant DE-FG02-01ER15173 (to R.A.B.). D.J.B. gratefully acknowledges funding from the Leverhulme Trust and Natural Environment Research Council (NE/E015190/1), and through a Royal Society-Wolfson Research Merit Award. M.P. acknowledges support from the Yale Climate and Energy Institute.

Author Contributions All four authors were involved in drafting the paper, led by M.P. K.C. and R.A.B. developed and applied procedures for modelling biotic weathering by land plants, and D.J.B. undertook the leaf-scale and global-scale simulations of vegetation processes.

Author Information Reprints and permissions information is available at www.nature.com/reprints. Correspondence and requests for materials should be addressed to M.P. (mark.pagani@yale.edu).

METHODS

Leaf gas exchange calculations. Effects of temperature and atmospheric CO_2 on rates of leaf photosynthesis and photorespiration (Supplementary Fig. 1) were calculated using a mechanistic model of leaf carbon assimilation[33], with maximum rates of carboxylation and electron transport of 63 μmol m^{-2} s^{-1} and 126 μmol m^{-2} s^{-1}, respectively. All calculations assumed a typical intercellular CO_2 concentration (0.7) multiplied by atmospheric CO_2 (ref. 34), with an irradiance of 1,000 μmol photons m^{-2} s^{-1}. The equations for rates of oxygenation and carboxylation (refs 26, 35) and the temperature sensitivities of relevant biochemical parameters[36] have previously been established.

The results of our leaf gas exchange calculations indicate a high sensitivity of photorespiratory CO_2 release rates to increases in temperature[35]. The calculations further show that high-temperature effects are greatest at low (200 p.p.m.) atmospheric CO_2 concentrations and become diminished as CO_2 concentrations increase (Supplementary Fig. 1). Overall, these results, and the biochemical rationale for them described in the main text, underpin our hypothesis that as atmospheric CO_2 concentrations decline towards 200 p.p.m. in the long-term, photorespiratory CO_2 releases increase, to an extent enhanced by climatic warming.

Sheffield Dynamic Global Vegetation Model simulations. The Sheffield Dynamic Global Vegetation Model (SDGVM) simulates global patterns of net primary production (NPP), leaf area index (LAI) and the distribution of plant functional types from monthly inputs of temperature, precipitation, relative humidity and cloudiness, and global data sets of soil texture[26,37]. Core modules of net photosynthesis, stomatal conductance, canopy transpiration, uptake of mineralized nitrogen and responses of these attributes to changes in soil water supply are detailed and rigorously evaluated against field observations[26,37]. A key feature of the model is the coupling of above- and belowground carbon and nitrogen cycles. Litter production influences soil carbon and nitrogen pools via the Century soil nutrient cycling model[38], which in turn feed back to influence aboveground primary production.

SDGVM local- and global-scale predictions of NPP, LAI and global plant functional type distributions have been extensively and successfully evaluated against a wide range of measurements and field observations[26]. SDGVM accurately reproduces actual site-specific observations and measurements of NPP and LAI for a range of forest types in the tropics and throughout Europe and North America[26,37]. Simulations forcing SDGVM with an observed (ISLSCP) and simulated (HadCM2) modern-day $1^\circ \times 1^\circ$ (latitude × longitude) climatology further indicate close global-scale agreement in both cases between calculated LAI values and satellite measurements of the normalized difference vegetation index, a measure of changes in the flux density of red light and far-red light[26]. The SDGVM-simulated geographical distribution of plant functional types is in close agreement with maps of 'actual' vegetation[26]. Global terrestrial NPP for the contemporary climate and CO_2 is estimated with SDGVM to be 62 Gt C yr^{-1}, in agreement with satellite-based estimates of about 55–60 Gt C yr^{-1} (ref. 39).

The sensitivity of NPP predictions of SDGVM to CO_2 and climate is similar to those of other dynamic vegetation models[40,41]. The CO_2 fertilization response of NPP compares favourably to that reported in Free Air Carbon Dioxide Enrichment experiments for temperate forested sites in North America and Italy; a 19% (model) versus a 23% (observed) increase between 367 and 550 p.p.m. (ref. 42).

Global simulations of the geographical distribution of plant functional types (which depends on NPP, LAI and minimum temperature thresholds) for the cool, low-CO_2 glacial climate of the last ice age are in general agreement with reconstructed vegetation patterns (geographical locations and areal extent) from palaeo-evidence at the global scale and from palynological evidence for North America[26]. Canopy LAI reductions and changes in forest cover in response to glacial CO_2 and climate are comparable to those of the TRIFFID[43] and BIOME3[44] dynamic global vegetation models. This indicates similar sensitivities to changes in the balance between canopy transpiration and NPP under a low atmospheric CO_2 concentration.

31. Berner, R. A. GEOCARBSULF; a combined model for Phanerozoic atmospheric O_2 and CO_2. *Geochim. Cosmochim. Acta* **70,** 5653–5664 (2006).
32. Volk, T. Feedbacks between weathering and atmospheric CO_2 over the last 100 million years. *Am. J. Sci.* **287,** 763–779 (1987).
33. Farquhar, G. D., von Caemmerer, S. & Berry, J. A. A biochemical model of photosynthetic CO_2 assimilation in leaves of C_3 species. *Planta* **149,** 78–90 (1980).
34. von Caemmerer, S. & Evans, J. R. Determination of the average partial pressure of CO_2 in chloroplasts from leaves of several C_3 plants. *Aust. J. Plant Physiol.* **18,** 287–305 (1991).
35. Sharkey, T. D. Estimating the rate of photorespiration in leaves. *Physiol. Plant.* **73,** 147–152 (1988).
36. Bernacchi, C. J., Singsaas, E. L., Pimentel, C., Portis, A. R. & Long, S. P. Improved temperature response functions for models of Rubisco-limited photosynthesis. *Plant Cell Environ.* **24,** 253–259 (2001).
37. Woodward, F. I., Smith, T. M. & Emanuel, W. R. A global land primary productivity and phytogeography model. *Glob. Biogeochem. Cycles* **9,** 471–490 (1995).
38. Parton, W. J. *et al.* Observations and modeling of biomass and soil organic matter dynamics for the grassland biome worldwide. *Glob. Biogeochem. Cycles* **7,** 785–809 (1993).
39. Running, S. W. *et al.* A continuous satellite-derived measure of global terrestrial primary production. *Bioscience* **54,** 547–560 (2004).
40. Hickler, T. *et al.* CO_2 fertilization in temperate FACE experiments not representative of boreal and tropical forests. *Glob. Change Biol.* **14,** 1–12 (2008).
41. Sitch, S. *et al.* Evaluation of the terrestrial carbon cycle, future plant geography and climate-carbon cycle feedbacks using five dynamic global vegetation models (SDGVMs). *Glob. Change Biol.* **14,** 2015–2039 (2008).
42. Woodward, F. I. & Kelly, C. K. Responses of global plant diversity capacity to changes in carbon dioxide concentration and climate. *Ecol. Lett.* **11,** 1229–1237 (2008).
43. Cowling, S. A. *et al.* Simulated glacial and interglacial vegetation across Africa: implications for species phylogenies and trans-African migration of plants and animals. *Glob. Change Biol.* **14,** 827–840 (2008).
44. Cowling, S. A., Maslin, M. A. & Sykes, M. T. Paleovegetation simulations of lowland Amazonia and implications for neotropical allopatry and speciation. *Quat. Res.* **55,** 140–149 (2001).